

**THE $b \rightarrow s\ell^+\ell^-$ ANOMALIES
AND
THEIR IMPLICATIONS FOR NEW PHYSICS**

S. DESCOTES-GENON

*Laboratoire de Physique Théorique, CNRS/Univ. Paris-Sud 11 (UMR 8627)
91405 Orsay Cedex, France*

L. HOFER ^a

*Department de Física Quàntica i Astrofísica (FQA)
Institut de Ciències del Cosmos (ICCUB)
Universitat de Barcelona (UB), Martí Franquès 1
08028 Barcelona, Spain*

J. MATIAS

*Universitat Autònoma de Barcelona
08193 Bellaterra, Spain*

J. VIRTO

*Theoretische Physik 1, Naturwissenschaftlich-Technische Fakultät
Universität Siegen, 57068 Siegen, Germany*

Recently, the LHC has found several anomalies in exclusive semileptonic $b \rightarrow s\ell^+\ell^-$ decays. In this proceeding, we summarize the most important results of our global analysis of the relevant decay modes. After a discussion of the hadronic uncertainties entering the theoretical predictions, we present an interpretation of the data in terms of generic new physics scenarios. To this end, we have performed model-independent fits of the corresponding Wilson coefficients to the data and have found that in certain scenarios the best fit point is preferred over the Standard Model by a global significance of more than 4σ . Based on the results, the discrimination between high-scale new physics and low-energy QCD effects as well as the possibility of lepton-flavour universality violation are discussed.

1 Introduction

The flavour-changing neutral current (FCNC) transition $b \rightarrow s\ell^+\ell^-$ can be probed through various decay channels, currently studied in detail at the LHCb, CMS and ATLAS experiments. Recent experimental results have shown interesting deviations from the SM: The LHCb analysis¹ of the 3fb^{-1} data on $B \rightarrow K^*\mu^+\mu^-$ in particular confirms a $\sim 3\sigma$ anomaly in two large-recoil bins of the angular observable $P_5^{\prime 2,3}$ that was already present in the 1fb^{-1} results presented in 2013⁴. The observable $R_K = Br(B \rightarrow K\mu^+\mu^-)/Br(B \rightarrow Ke^+e^-)$ was measured by LHCb⁵ in the dilepton mass range from 1 to 6 GeV^2 as $0.745_{-0.074}^{+0.090} \pm 0.036$, corresponding to a 2.6σ tension with its SM value predicted to be equal to 1 (to a very good accuracy). Finally, also the LHCb results⁶ on the branching ratio of $B_s \rightarrow \phi\mu^+\mu^-$ exhibit deviations at the $\sim 3\sigma$ level in two large-recoil bins.

^aSpeaker

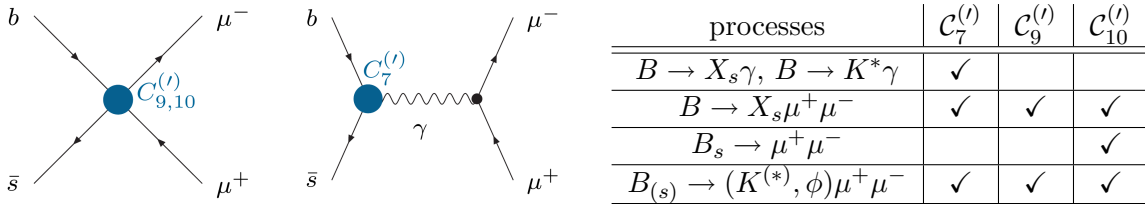


Figure 1 – Effective couplings $\mathcal{C}_{7,9,10}^{(\prime)}$ contributing to $b \rightarrow s \ell^+ \ell^-$ transitions and sensitivity of the various radiative and (semi-)leptonic $B_{(s)}$ decays to them.

The appearance of several tensions in different $b \rightarrow s \ell^+ \ell^-$ channels is quite intriguing because all these observables are sensitive to the same effective couplings $\mathcal{C}_{7,9,10}^{(\prime)}$ illustrated in Fig. 1 and induced by the operators

$$\begin{aligned}
 \mathcal{O}_9^{(\prime)} &= \frac{\alpha}{4\pi} [\bar{s} \gamma^\mu P_{L(R)} b] [\bar{\mu} \gamma_\mu \mu], & \mathcal{O}_{10}^{(\prime)} &= \frac{\alpha}{4\pi} [\bar{s} \gamma^\mu P_{L(R)} b] [\bar{\mu} \gamma_\mu \gamma_5 \mu], \\
 \mathcal{O}_7^{(\prime)} &= \frac{\alpha}{4\pi} m_b [\bar{s} \sigma_{\mu\nu} P_{R(L)} b] F^{\mu\nu}, & &
 \end{aligned} \tag{1}$$

where $P_{L,R} = (1 \mp \gamma_5)/2$ and m_b denotes the b quark mass. It is thus natural to ask whether a new physics contribution to these couplings could simultaneously account for the various tensions in the data. Beyond the SM, contributions to $\mathcal{C}_{9,10}^{(\prime)}$ are for instance generated at tree level in scenarios with Z' bosons or lepto-quarks. Note that additional scalar or pseudoscalar couplings $\mathcal{C}_{S,S',P,P'}$ cannot address the above-mentioned anomalies since their contributions are suppressed by small lepton masses. Therefore we will not discuss this possibility in the following.

The parameter space spanned by the couplings $\mathcal{C}_{7,9,10}^{(\prime)}$ is probed through various observables in radiative and (semi-)leptonic $B_{(s)}$ decays, each of them sensitive to a different subset of coefficients (see Fig. 1). A complete investigation of potential new physics effects thus requires a combined study of these observables including correlations among them. The first analysis in this spirit, performed in Ref. ⁷ with the data of 2013, pointed to a large negative contribution to the Wilson coefficient \mathcal{C}_9 . This general picture was confirmed later on by other groups, using different/additional observables, different theoretical input for the form factors etc. (e.g. Refs. ^{8,9}). In this proceeding, we report the most important results of our analysis in Ref. ¹⁰ which can be compared to other recent global analyses ^{11,12,13} and which improves the original study in Ref. ⁷ in many aspects: It includes the latest experimental results of all relevant channels, uses refined techniques to estimate uncertainties originating from power corrections to the hadronic form factors and from non-perturbative charm loops, and consistently takes into account experimental and theoretical correlations.

Before presenting the results from our fits in Sec. 3, with a special emphasis on the possibility of discriminating between high-scale new physics and low-energy QCD effects as well as on the possibility of lepton-flavour universality violation, we discuss in Sec. 2 the hadronic uncertainties entering the theoretical predictions of the relevant observables. Our conclusions are given in Sec. 4.

2 Hadronic uncertainties

Predictions for exclusive semileptonic B decays are plagued by QCD effects of perturbative and non-perturbative nature. At leading order (LO) in the effective theory, predictions involve tree-level diagrams with insertions of the operators $\mathcal{O}_{7,9,10}$ (generated at one loop in the SM), as well as one-loop diagrams with an insertion of the charged-current operator $\mathcal{O}_2 = [\bar{s} \gamma^\mu P_L c] [\bar{c} \gamma_\mu P_L b]$ (generated at tree level in the SM). In contributions of the first type, the leptonic and the hadronic current factorize, and QCD corrections are constrained to the hadronic $B \rightarrow M$ current (first two diagrams in Fig. 2). This class of *factorizable QCD corrections* thus forms part of the

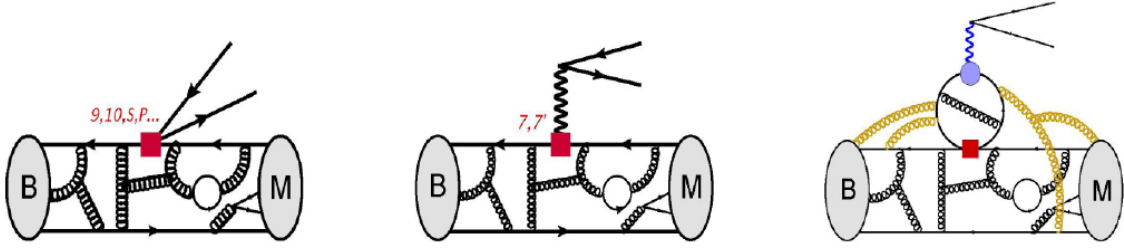


Figure 2 – Illustration of factorizable (first two diagrams) and non-factorizable (third diagram) QCD corrections to exclusive $B \rightarrow M \ell^+ \ell^-$ matrix elements.

hadronic form factors parametrizing the $B \rightarrow M$ transition. Contributions of the second type, on the other hand, receive *non-factorizable QCD corrections* (third diagram in Fig. 2) that cannot be absorbed into form factors. In the following we discuss the uncertainties stemming from the two types of corrections and their implementation in our analysis.

2.1 Form factor uncertainties

The form factors are available from lattice as well as from light-cone sum rule (LCSR) calculations, with the former being suited for the region of high $q^2 > 15 \text{ GeV}^2$ and the latter for the region of low $q^2 < 8 \text{ GeV}^2$. Since the form factors introduce a dominant source of uncertainties into the theory predictions, it is desirable to reduce the sensitivity to them as much as possible. For $B \rightarrow V \ell^+ \ell^-$ decays, with V being a vector meson, this can be achieved in the low- q^2 region by exploiting large-recoil symmetries of QCD. At LO in α_s and Λ/m_b , these symmetries enforce certain relations among the seven hadronic form factors V , A_1 , A_2 , A_0 , T_1 , T_2 , T_3 , like e.g.

$$\frac{m_B(m_B + m_{K^*})A_1 - 2E(m_B - m_{K^*})A_2}{m_B^2 T_2 - 2Em_B T_3} = 1 + \mathcal{O}(\alpha_s, \Lambda/m_b), \quad (2)$$

where m_B denotes the mass of the B meson, and m_{K^*} and E the mass and the energy of the K^* meson. From the experimentally measured coefficients of the differential angular distribution of $B \rightarrow V \ell^+ \ell^-$, one can construct observables that involve ratios like the one in eq. (2). The resulting observables $P_i^{(\prime)}$ then only exhibit a mild form factor dependence, suppressed by powers of α_s and Λ/m_b .

For the cancellation of the form factor uncertainties in ratios like the one in eq. (2), it is crucial to have control of the correlations among the errors of the different form factors. These correlations can be taken into account via two orthogonal approaches: Either they can be assessed directly from the LCSR calculation (Ref. ¹⁴ provides LCSR form factors with correlation matrices), or they can be implemented resorting to the large-recoil symmetry relations. Whereas the former method is limited to the particular set of LCSR form factors from Ref. ¹⁴ and hence sensitive to details of the corresponding calculation, the latter method determines the correlations in a model-independent way from first principles and can thus also be applied to different sets of form factors like the ones from Ref. ¹⁵. As a drawback, correlations are obtained from large-recoil symmetries only up to Λ/m_b corrections which have to be estimated. For the estimate of these *factorizable power corrections*, we follow the strategy developed in Ref. ¹⁶, which is based on and further refines a method first proposed in Ref. ¹⁷.

2.2 Uncertainties from $c\bar{c}$ loops

Long-distance charm-loop effects (third diagram in Fig. 2) can mimic the effect of an effective coupling $\mathcal{C}_9^{c\bar{c}}$. Due to the non-local structure of these corrections, their contribution is expected to have a non-constant q^2 -dependence, where q^2 is the squared invariant masses of the lepton

Coefficient	Best fit	1σ	3σ	Pull _{SM}
$\mathcal{C}_7^{\text{NP}}$	-0.02	[-0.04, -0.00]	[-0.07, 0.03]	1.2
$\mathcal{C}_9^{\text{NP}}$	-1.09	[-1.29, -0.87]	[-1.67, -0.39]	4.5
$\mathcal{C}_{10}^{\text{NP}}$	0.56	[0.32, 0.81]	[-0.12, 1.36]	2.5
$\mathcal{C}_{7'}^{\text{NP}}$	0.02	[-0.01, 0.04]	[-0.06, 0.09]	0.6
$\mathcal{C}_{9'}^{\text{NP}}$	0.46	[0.18, 0.74]	[-0.36, 1.31]	1.7
$\mathcal{C}_{10'}^{\text{NP}}$	-0.25	[-0.44, -0.06]	[-0.82, 0.31]	1.3
$\mathcal{C}_9^{\text{NP}} = \mathcal{C}_{10}^{\text{NP}}$	-0.22	[-0.40, -0.02]	[-0.74, 0.50]	1.1
$\mathcal{C}_9^{\text{NP}} = -\mathcal{C}_{10}^{\text{NP}}$	-0.68	[-0.85, -0.50]	[-1.22, -0.18]	4.2
$\mathcal{C}_9^{\text{NP}} = -\mathcal{C}_{9'}^{\text{NP}}$	-1.06	[-1.25, -0.85]	[-1.60, -0.40]	4.8

Table 1: Results of various one-parameter fits for the Wilson coefficients $\{\mathcal{C}_i\}$.

pair. Together with the perturbative SM contribution $\mathcal{C}_{9\text{SMpert}}^{\text{eff}}$ and a potential constant NP coupling $\mathcal{C}_9^{\text{SM}}$, it can be cast into an effective Wilson coefficient

$$\mathcal{C}_9^{\text{eff } i}(q^2) = \mathcal{C}_{9\text{SMpert.}}^{\text{eff}}(q^2) + \mathcal{C}_9^{\text{NP}} + \mathcal{C}_9^{c\bar{c}i}(q^2), \quad (3)$$

with a different $\mathcal{C}_9^{c\bar{c}i}$ and hence also a different $\mathcal{C}_9^{\text{eff } i}$ for the three transversity amplitudes $i = 0, \parallel, \perp$. Currently, only a partial calculation¹⁵ exists, yielding values $\mathcal{C}_{9\text{KMPW}}^{c\bar{c}i}$ that tend to enhance the anomalies. In our analysis, we assume that this partial result is representative for the order of magnitude of the total charm-loop contribution and we assign an error to unknown charm-loop effects varying

$$\mathcal{C}_9^{c\bar{c}i}(q^2) = s_i \mathcal{C}_{9\text{KMPW}}^{c\bar{c}i}(q^2), \quad \text{for } -1 \leq s_i \leq 1. \quad (4)$$

3 Results of the global fit

Our reference fits are obtained using the following experimental input: branching ratios and angular observables of the decays $B \rightarrow K^* \mu^+ \mu^-$ and $B_s \rightarrow \phi \mu^+ \mu^-$, branching ratios of the charged and neutral modes $B \rightarrow K \mu^+ \mu^-$, the branching ratios of $B \rightarrow X_s \mu^+ \mu^-$, $B_s \rightarrow \mu^+ \mu^-$ and $B \rightarrow X_s \gamma$, as well as the isospin asymmetry A_I and the time-dependent CP asymmetry $S_{K^* \gamma}$ of $B \rightarrow K^* \gamma$. For the theoretical predictions, we use lattice form factors from Refs.^{18,19} in the low-recoil region, and LCSR form factors from Ref.¹⁵ (except for $B_s \rightarrow \phi$ where Ref.¹⁴ is used), with correlations assessed from the large-recoil symmetries.

Starting from a model hypothesis with n free parameters for the Wilson coefficients $\{\mathcal{C}_i^{\text{NP}}\}$, we then perform a frequentist $\Delta\chi^2$ -fit, including experimental and theoretical correlation matrices. In Tab. 1 we show our results for various one-parameter scenarios. In the last column we give the SM-pull for each scenario, i.e. we quantify by how many sigma the best fit point is preferred over the SM point $\{\mathcal{C}_i^{\text{NP}}\} = 0$ in the given scenario. A scenario with a large SM-pull thus allows for a big improvement over the SM and a better description of the data. From the results in Tab. 1 we infer that a large negative $\mathcal{C}_9^{\text{NP}}$ is required to explain the data, with $\mathcal{C}_9^{\text{NP}} \sim -1.1$ in the scenario where only this coefficient is generated. A decomposition into the different exclusive decay channels, as well as into low- and large-recoil regions, shows that each of these individual contributions points to the same solution, i.e. a negative $\mathcal{C}_9^{\text{NP}}$, albeit with varying significance. We refer the reader to Ref.¹⁰ for further results, e.g. for fits in various 2-parameter scenarios as well as for the full 6-parameter fit of $\mathcal{C}_{7,9,10}^{(\prime)\text{NP}}$ resulting in a SM-pull of 3.6σ .

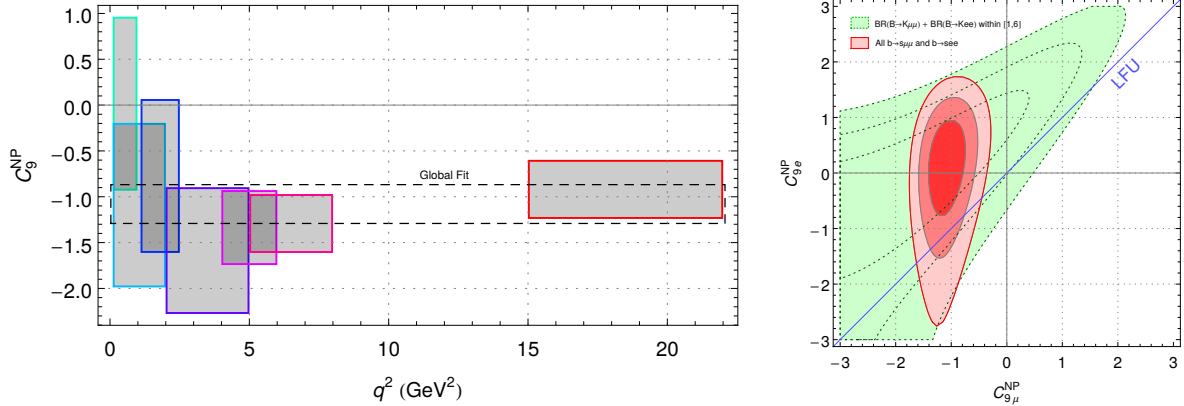


Figure 3 – Left: Bin-by-bin fit of the one-parameter scenario with a single coefficient C_9^{NP} . Right: Fit with independent coefficients $C_{9\mu}^{\text{NP}}$ and C_{9e}^{NP} .

3.1 New physics vs. non-perturbative charm-contribution

According to Eq. (3), a potential NP contribution C_9^{NP} enters amplitudes always together with a charm-loop contribution $C_9^{c\bar{c}i}(q^2)$, spoiling an unambiguous interpretation of the fit result from the previous section in terms of new physics. However, whereas C_9^{NP} does not depend on the squared invariant mass q^2 of the lepton pair, $C_9^{c\bar{c}i}(q^2)$ is expected to exhibit a non-trivial q^2 -dependence. Following Ref. ¹², we show in Fig. 3 on the left a bin-by-bin fit for the one-parameter scenario with a single coefficient C_9^{NP} . The results obtained in the individual bins are consistent with each other, allowing thus for a solution C_9^{NP} that is constant in the whole q^2 region, as required for an interpretation in terms of new physics, though the situation is not conclusive due to the large uncertainties in the single bins.

An alternative strategy to address this question, consists in a direct fit of the q^2 -dependent charm contribution $C_9^{c\bar{c}i}(q^2)$, as performed in Ref. ²⁰ using a parametrization which introduces 18 free parameters. Given the large number of free parameters, it is neither surprising that a good fit to the data can be achieved in this way, nor that one of the 12 parameters encoding a non-trivial q^2 -dependence fluctuates from zero by $\gtrsim 2\sigma$. Therefore, the results obtained in Ref. ²⁰ do not disfavour a q^2 -independent NP solution C_9^{NP} . A solid interpretation of the results in Ref. ²⁰ would require a comparison of the goodness of the 18-parameter fit for $C_9^{c\bar{c}i}(q^2)$ with the 1-parameter fit for C_9^{NP} , taking into account the different number of degrees of freedom, a task that has not been undertaken in Ref. ²⁰.

3.2 Lepton-flavour universality violation

Since the measurement of R_K suggests the violation of lepton-flavour universality, we also studied the situation where the muon- and the electron-components of the operators $C_{9,10}^{(\prime)}$ receive independent new physics contributions $C_{i\mu}^{\text{NP}}$ and C_{ie}^{NP} , respectively. The electron-couplings C_{ie}^{NP} are constrained by adding the decays $B \rightarrow K^{(*)}e^+e^-$ to the global fit. Note that the correlated fit to $B \rightarrow K\mu^+\mu^-$ and $B \rightarrow Ke^+e^-$ simultaneously is equivalent to a direct inclusion of the observable R_K .

In Fig. 3 on the right we display the result for the two-parameter fit to the coefficients $C_{9\mu}^{\text{NP}}$ and C_{9e}^{NP} . The fit prefers an electron-phobic scenario with new physics coupling to $\mu^+\mu^-$ but not to e^+e^- . Under this hypothesis, that should be tested by measuring R_{K^*} and R_ϕ , the SM-pull increases by $\sim 0.5\sigma$ compared to the value in Tab. 1 for the lepton-flavour universal scenario.

4 Conclusions

LHCb data on $b \rightarrow s\ell^+\ell^-$ decays shows several tensions with SM predictions, in particular in the angular observable P'_5 of $B \rightarrow K^*\mu^+\mu^-$, in the branching ratio of $B_s \rightarrow \phi\mu^+\mu^-$, and in the ratio $R_K = Br(B \rightarrow K\mu^+\mu^-)/Br(B \rightarrow Ke^+e^-)$ (all of them at the $\sim 3\sigma$ level). In global fits of the Wilson coefficients to the data, scenarios with a large negative C_9^{NP} are preferred over the SM by typically more than 4σ . A bin-by-bin analysis demonstrates that the fit is compatible with a q^2 -independent effect generated by high-scale new physics, though a q^2 -dependent QCD effect cannot be excluded with current precision. Note, however, that a QCD effect could not explain the tension in R_K . The latter observable further favours a lepton-flavour violating scenario with new physics coupling only to $\mu^+\mu^-$ but not to e^+e^- , a scenario to be probed by a measurement of the analogous ratios R_{K^*} and R_ϕ to probe this hypothesis.

Acknowledgments

L.H. is grateful to the organizers for the invitation to the workshop and thanks the participants for stimulating discussions. The work of L.H. was supported by the grants FPA2013-46570-C2-1-P and 2014-SGR-104, and partially by the Spanish MINECO under the project MDM-2014-0369 of ICCUB (Unidad de Excelencia “María de Maeztu”). JV is funded by the DFG within research unit FOR 1873 (QFET), and acknowledges financial support from CNRS. SDG, JM and JV acknowledge financial support from FPA2014-61478-EXP.

References

1. R. Aaij *et al.* [LHCb Collaboration], arXiv:1512.04442 [hep-ex].
2. S. Descotes-Genon, J. Matias, M. Ramon and J. Virto, JHEP **1301** (2013) 048, arXiv:1207.2753 [hep-ph].
3. S. Descotes-Genon, T. Hurth, J. Matias and J. Virto, JHEP **1305** (2013) 137, arXiv:1303.5794 [hep-ph].
4. LHCb Collaboration, PRL **111** (2013) 191801, arXiv:1308.1707 [hep-ex].
5. LHCb Collaboration, Phys. Rev. Lett. **113** (2014) 151601, arXiv:1406.6482 [hep-ex].
6. LHCb Collaboration, JHEP **1307** (2013) 084, arXiv:1305.2168 [hep-ex].
7. S. Descotes-Genon, J. Matias and J. Virto, Phys. Rev. D **88** (2013) 074002, arXiv:1307.5683 [hep-ph].
8. W. Altmannshofer and D. M. Straub, Eur. Phys. J. C **73** (2013) 2646 arXiv:1308.1501 [hep-ph].
9. F. Beaujean, C. Bobeth and D. van Dyk, Eur. Phys. J. C **74** (2014) 2897 [Eur. Phys. J. C **74** (2014) 3179], arXiv:1310.2478 [hep-ph].
10. S. Descotes-Genon, L. Hofer, J. Matias and J. Virto, arXiv:1510.04239 [hep-ph].
11. W. Altmannshofer and D. M. Straub, Eur. Phys. J. C **75** (2015) 8, 382, arXiv:1411.3161 [hep-ph].
12. W. Altmannshofer and D. M. Straub, arXiv:1503.06199 [hep-ph].
13. T. Hurth, F. Mahmoudi and S. Neshatpour, arXiv:1603.00865 [hep-ph].
14. A. Bharucha, D. M. Straub and R. Zwicky, arXiv:1503.05534 [hep-ph].
15. A. Khodjamirian, T. Mannel, A. A. Pivovarov and Y.-M. Wang, JHEP **1009** (2010) 089, arXiv:1006.4945 [hep-ph].
16. S. Descotes-Genon, L. Hofer, J. Matias and J. Virto, JHEP **1412** (2014) 125, arXiv:1407.8526 [hep-ph].
17. S. Jäger and J. Martin Camalich, JHEP **1305** (2013) 043, arXiv:1212.2263 [hep-ph].
18. R. R. Horgan, Z. Liu, S. Meinel and M. Wingate, Phys. Rev. D **89** (2014) 9, 094501, arXiv:1310.3722 [hep-lat], PoS LATTICE **2014** (2015) 372, arXiv:1501.00367 [hep-lat].

19. C. Bouchard *et al.* [HPQCD Collaboration], Phys. Rev. D **88** (2013) 5, 054509 [Phys. Rev. D **88** (2013) 7, 079901], arXiv:1306.2384 [hep-lat].
20. M. Ciuchini *et al.* , arXiv:1512.07157 [hep-ph].